Article

Highly Active and Durable Rh−Mo-Based Catalyst for the NO−CO−C$_3$H$_6$−O$_2$ Reaction Prepared by Using Hybrid Clustering

Shun Hayashi,* Shinji Endo, Hiroki Miura, and Tetsuya Shishido*

Read Online

ACCESS | Metrics & More | Article Recommendations | Supporting Information

ABSTRACT: We developed a method for preparing catalysts by using hybrid clustering to form a high density of metal/oxide interfacial active sites. A Rh−Mo hybrid clustering catalyst was prepared by using a hybrid cluster, $[(RhCp^*)_4Mo_4O_{16}]$ ($Cp^* = \eta^5\text{-}C_5Me_5$), as the precursor. The activities of the Rh−Mo catalysts toward the NO−CO−C$_3$H$_6$−O$_2$ reaction depended on the mixing method (hybrid clustering > coimpregnation ≈ pristine Rh). The hybrid clustering catalyst also exhibited high durability against thermal aging at 1273 K in air. The activity and durability were attributed to the formation of a high-density of Rh/MoO$_x$ interfacial sites. The NO reduction mechanism on the hybrid clustering catalyst was different from that on typical Rh catalysts, where the key step is the N−O cleavage of adsorbed NO. The reducibility of the Rh/MoO$_x$ interfacial sites

NO-CO-C$_3$H$_6$-O$_2$ reaction over Rh-Mo/Al$_2$O$_3$

Hybrid clustering

Coimpregnation

contributed to the partial oxidation of C$_3$H$_6$ to form acetate species, which reacted with NO+O$_2$ to form N$_2$ via the adsorbed NCO species. The formation of reduced Rh on Rh$_4$Mo$_4$/Al$_2$O$_3$ was not as essential as that on typical Rh catalysts; this explained the improvement in durability.

KEYWORDS: *hybrid clustering, organometallic polyoxometalate, automotive catalysts, nanoparticles, interface, rhodium*
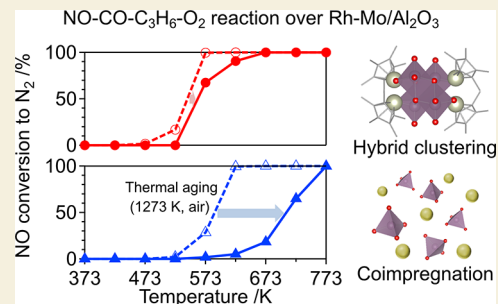
1. INTRODUCTION

Three-way catalysts (TWCs), which remove major pollutants, such as carbon monoxide (CO), hydrocarbons (HC), and nitrogen oxides (NO$_x$), from exhaust emissions play an important role in automotive pollution control.[1−4] Among the platinum group metal (PGM) elements frequently used as a key component of TWCs, Rh has been regarded as an essential element because of its efficiency in reducing NO$_x$ to N$_2$. Because PGMs are scarce and expensive, a catalyst design for maximizing their use is required.

The development of support materials has improved the activity and durability of TWCs. TWCs are usually prepared by the impregnation method. In this method, PGM precursors are deposited on a support and calcined to form PGM nanoparticles. Metal oxides are used as supports because of their high thermal stability. Since the PGM nanoparticles are responsible for the reaction, metal dispersion is a critical factor for determining the performance. The metal/support interface plays an important role in inhibiting aggregation by stabilizing the metal species.[5−8] Although the activity of TWCs is derived from PGMs, the development of PGM precursors has received limited attention.[9,10] Precursors are typically monomeric compounds, such as chlorides and nitrate salts. This is because the type of precursor has little effect on the activity under harsh reaction conditions.[11]

We had previously reported a catalyst preparation method; namely hybrid clustering, for the efficient formation of metal/oxide interfacial active sites.[12] Hybrid clusters or organo-

metallic polyoxometalates, formulated as $[(M^1L)_xM_y^2O_n]$, are composed of metal ions (M^1), metal oxide clusters ($M_y^2O_n$), and organic ligands (L).[13] Because the surface oxygen atoms of the metal oxide clusters are coordinated to the metal ions, the hybrid clusters can be considered as the minimal building blocks with a metal/oxide interface. Therefore, we predicted that catalysts prepared from hybrid clusters would comprise a high density of metal/oxide interfaces, contributing to the formation of unique catalytic active sites (Figure 1). Although hybrid clusters have potential for such applications, there have been few reports on their use in heterogeneous catalysts.[14,15]
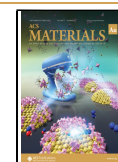
In this study, we prepared Rh−M catalysts (M = V and Mo) by using hybrid clustering. The hybrid clustering catalysts displayed higher activities for TWC reactions than the Rh-based coimpregnated catalysts or pristine Rh catalysts. In addition, the durability of the Rh−Mo-based hybrid clustering catalyst against thermal aging was considerably improved.
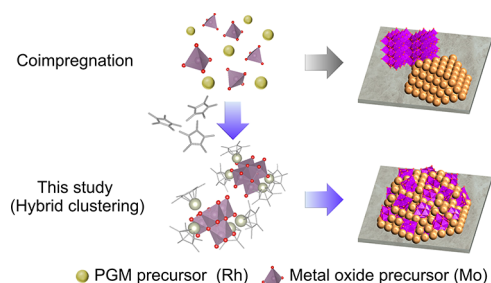
Figure 1. High-density formation of metal/oxide interfacial site through hybrid clustering.

2. RESULTS AND DISCUSSION

2.1. Catalyst Preparation and Characterization

The hybrid clustering catalysts, Rh_4Mo_4/Al_2O_3 and Rh_4V_6/Al_2O_3, were prepared by using $[(RhCp^*)_4Mo_4O_{16}]$ and $[(RhCp^*)_4V_6O_{19}]$ ($Cp^* = \eta^5$-C_5Me_5), respectively, as the catalyst precursors. These precursors were synthesized as per procedures used in previous studies[16,17] and characterized by Fourier transform infrared (FT-IR) and ^1H and $^{13}C\{^1H\}$ NMR spectroscopy (Figures S1 and S2). After the precursor clusters were adsorbed onto γ-Al_2O_3 via impregnation with methanol, the catalysts were prepared by performing calcination under air flow at 773 K. Coimpregnated Rh−Mo and Rh−V catalysts, Rh−Mo/Al_2O_3 and Rh−V/Al_2O_3, and a pristine Rh catalyst, Rh/Al_2O_3, were prepared as references from $RhCl_3$, $(NH_4)_6[Mo_7O_{24}]\cdot4H_2O$, and NH_4VO_3 under identical calcination conditions.

Based on high-angle annular dark-field scanning transmission electron microscopy (HAADF-STEM) analysis, the average diameter of Rh_4Mo_4/Al_2O_3 was estimated to be 3.0 ± 0.9 nm (Figure 2a). Energy-dispersive X-ray spectroscopy
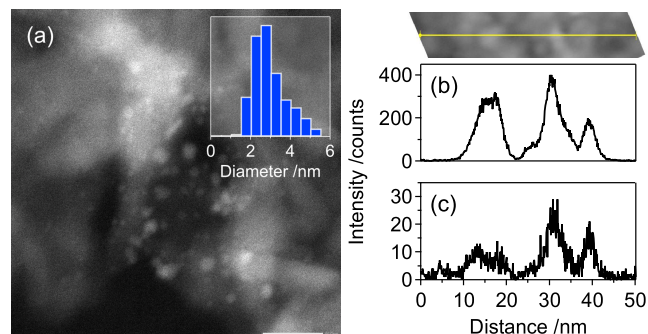
Figure 2. (a) HAADF-STEM image of Rh_4Mo_4/Al_2O_3 (scale bar = 10 nm). EDS line scan analysis of (b) Rh (Rh Lα) and (c) Mo (Mo Kα). A yellow line on the upper-right panel indicates the scanning positions.

(EDS) analysis revealed that the distributions of Rh and Mo overlapped well, suggesting that the nanoparticles were composed of both Rh and Mo (Figure 2b,c).

X-ray absorption near-edge structure analysis (XANES) was used to evaluate the electronic structures of Rh and Mo. The Rh K-edge XANES spectra revealed that the Rh species in both Rh_4Mo_4/Al_2O_3 and Rh−Mo/Al_2O_3 were Rh^{3+} (Figure 3a). The Fourier transform extended X-ray absorption fine structure (FT-EXAFS) spectra of the catalysts showed no peaks derived from the second coordination sphere, implying that the local structures of Rh were disordered (Figure S3).
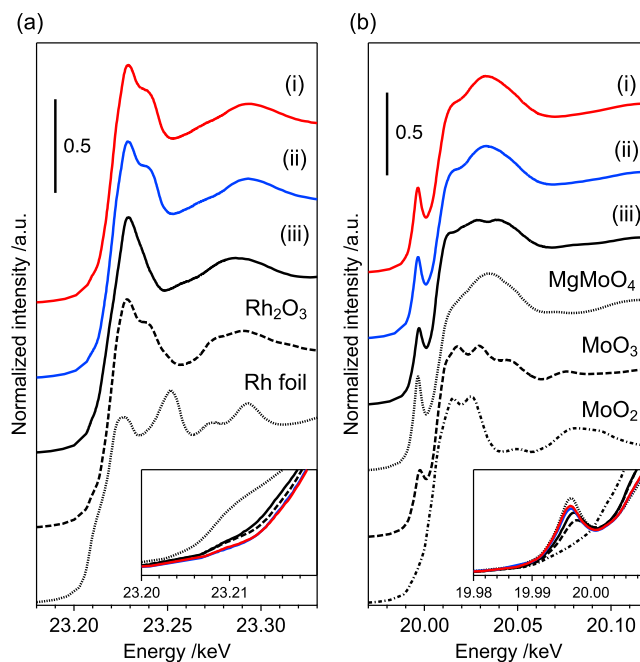

Figure 3. (a) Rh K- and (b) Mo K-edge XANES spectra of (i) Rh_4Mo_4/Al_2O_3, (ii) Rh−Mo/Al_2O_3, and (iii) $[(RhCp^*)_4Mo_4O_{16}]$. The spectra of (i) and (ii) closely overlap in the insets.

Because the pre-edge peaks in the Mo K-edge spectra were assigned to weak quadrupole-allowed (1s → 4d) and strong dipole-allowed (1s → 5p) transitions, the local structural disorder of the Mo oxide species reflects the intensity. The perfect octahedral symmetry only permits the quadrupole transition, while the structural disorder to distorted octahedral, square pyramidal, and tetrahedral symmetries promotes dipole-allowed transitions.[18,19] The Mo K-edge spectrum of Rh_4Mo_4/Al_2O_3 matched well that of Rh−Mo/Al_2O_3, implying that the local structure of Mo was independent of the preparation method. The pre-edge peak intensity of Rh_4Mo_4/Al_2O_3 was larger than that of the precursor $[(RhCp^*)_4Mo_4O_{16}]$, suggesting that structural distortion of the octahedral MoO_6 unit occurred during catalyst preparation (Figure 3b). These findings imply that the electronic and local structures of Rh and Mo are independent of the catalyst preparation technique used.

In contrast, the local structure of Rh evaluated by diffuse reflectance infrared Fourier transform (DRIFT) spectroscopy of adsorbed CO species depends on the catalyst preparation method (Figure 4). The doublet peaks observed for Rh_4Mo_4/Al_2O_3 corresponded to symmetric (2096 cm^{-1}) and asymmetric (2026 cm^{-1}) stretches of the geminal dicarbonyl species
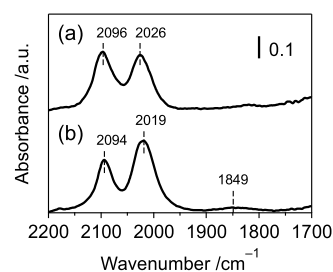
Figure 4. DRIFT spectra of adsorbed CO species on (a) Rh_4Mo_4/Al_2O_3 and (b) Rh−Mo/Al_2O_3.
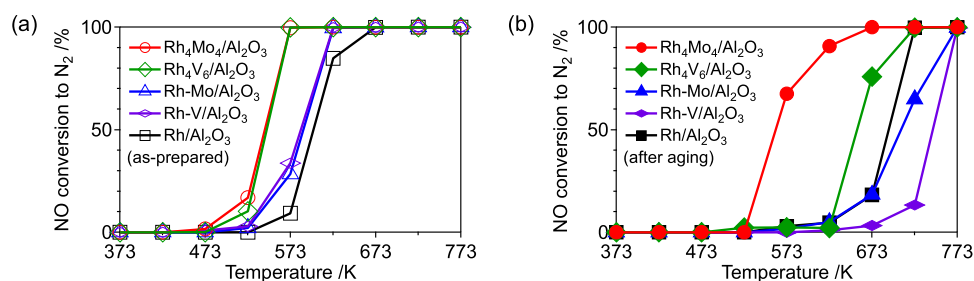
Figure 5. NO conversion to N_2 in $NO-CO-C_3H_6-O_2$ over the (a) as-prepared catalysts and (b) catalysts after thermal aging (1273 K, 5 h, air). Reaction condition: catalyst (200 mg) and total flow rate (100 mL min^{-1}). Gas composition: NO (1000 ppm), CO (1000 ppm), C_3H_6 (250 ppm), and O_2 (1125 ppm) balanced with He.

$Rh(CO)_2$.[20,21] This was also observed for $Rh-Mo/Al_2O_3$ (2094 and 2019 cm^{-1}). No peak assigned to linear $Rh-CO$ (2070 cm^{-1}) was observed, whereas a small peak assigned to bridged $Rh_2(CO)$ (1849 cm^{-1}) was observed only for $Rh-Mo/Al_2O_3$. The ratio of the integrated absorbance of symmetric and asymmetric stretches for $Rh(CO)_2$ (A_{as}/A_s) is related to the angle between the two CO groups.[8,22] For supported Rh-based catalysts, an atomically dispersed Rh species shows an angle of $\sim 90°$, while a Rh nanoparticle shows an angle of $\sim 120°$. The angles were estimated to be 89 and 112° for Rh_4Mo_4/Al_2O_3 and $Rh-Mo/Al_2O_3$, respectively (Figure S4, Table S1). This implies that Rh atoms in Rh_4Mo_4/Al_2O_3 were highly dispersed in Rh−Mo mixed nanoparticles, whereas the coimpregnation method afforded a typical Rh nanoparticle catalyst.

2.2. Activity for $NO-CO-C_3H_6-O_2$ Reactions

The activities of the catalysts were evaluated using $NO-CO-C_3H_6-O_2$ reactions. When the reaction was catalyzed by Rh_4Mo_4/Al_2O_3, the reduction of NO to N_2 started at 527 K, and a complete reduction of NO to N_2 was observed at 573 K ($T_{50} \sim 543$ K) (Figure 5a). This contrasts with $Rh-Mo/Al_2O_3$ and Rh/Al_2O_3, where the reaction started at 573 K ($T_{50} \sim 588$ and 600 K, respectively). In these catalysts, the conversion of CO proceeded prior to that of NO and C_3H_6 (Figure S5). In addition, the conversion of NO to N_2 in $NO-C_3H_6-O_2$ over Rh_4Mo_4/Al_2O_3 showed a similar trend to that of $NO-CO-C_3H_6-O_2$ (Figure S6). These findings imply that under the conditions of $NO-CO-C_3H_6-O_2$, C_3H_6 is responsible for NO reduction. The durability of the catalysts is discussed based on their activity after thermal aging at 1273 K for 5 h in air. Activity was assessed without regeneration (reduction). Although significant activity loss was observed for $Rh-Mo/Al_2O_3$ and Rh/Al_2O_3 ($T_{50} \sim 707$ and 693 K, respectively), only a slight decrease in the activity was observed for Rh_4Mo_4/Al_2O_3 ($T_{50} \sim 560$ K) (Figure 5b). In the case of the Rh−V-based catalysts, Rh_4V_6/Al_2O_3 showed higher activity than Rh−V/Al_2O_3 (Figure 5a). In contrast, a significant activity loss after thermal aging was observed for both Rh_4V_6/Al_2O_3 and $Rh-V/Al_2O_3$ (Figure 5b). This indicates that the introduction of either Mo or V by hybrid clustering contributes to the improvement of activity, whereas the effect on durability is limited to Mo. This implies the importance of combining Rh and Mo as well as the catalyst preparation method.

## 2.3. Origin of High Activity and Durability

The electronic structures of Rh_4Mo_4/Al_2O_3 and $Rh-Mo/Al_2O_3$ after the reaction were studied by using Rh K- and Mo K-edge XANES analyses. After the $NO-CO-C_3H_6-O_2$ reaction at 773 K for 1 h, the catalyst was cooled to room

temperature under He flow, exposed to air, and pelletized for XAS analysis. A red shift of both Rh K- and Mo K-edge spectra was observed for both catalysts, implying that the reduction of both Rh^{3+} and Mo^{6+} slightly progressed during the reaction, regardless of the catalyst preparation method (Figure 6). The
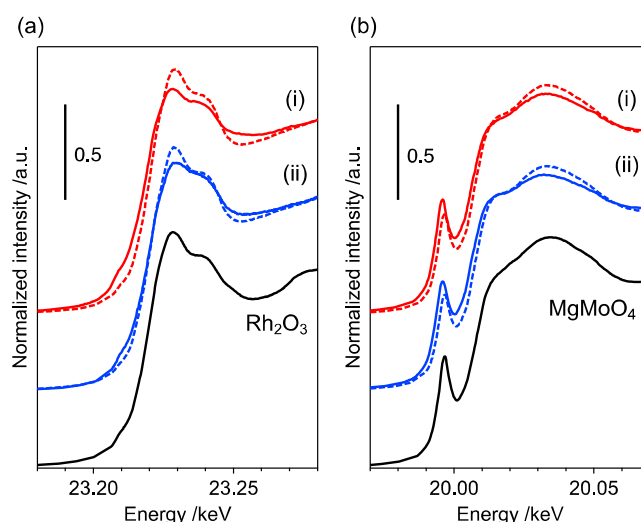
Figure 6. (a) Rh K- and (b) Mo K-edge XANES spectra of (i) Rh_4Mo_4/Al_2O_3 and (ii) $Rh-Mo/Al_2O_3$ before (dotted line) and after (solid line) the $NO-CO-C_3H_6-O_2$ reaction at 773 K.

interaction of the catalysts with CO was examined by transient response using mass spectrometry (MS). The switch from He to CO/He (1000 ppm) flow resulted in the immediate formation of CO_2 but the concentration decreased over time (Figure 7). This behavior implies that CO_2 was formed by the reaction of CO with the oxygen atom in the catalyst and not by the disproportionation of CO (2 CO → CO_2 + C). Therefore, the amount of CO_2 is a measure of the reducibility of the active phase or ease of oxygen vacancy formation. The formation of CO_2 was observed at 573 K for $Rh-Mo/Al_2O_3$ and Rh/Al_2O_3. No significant difference was found in the amount of CO_2 estimated from the peak area (Table S2), implying that the oxygen atom used for CO_2 formation was derived from Rh species, and the introduction of Mo by coimpregnation did not affect the reducibility. In contrast, the formation of CO_2 was observed at a lower temperature (473 K) for Rh_4Mo_4/Al_2O_3, and the amount of CO_2 formed at 573 K was much larger than that of the reference catalysts. This suggests that the oxygen atoms used for CO_2 formation were derived from Rh/MoO_x interfacial sites. The relative ratio of CO_2 to Rh in the catalyst (n_{CO_2}/n_{Rh}) was estimated to be 2.54 at 573 K (Table S2). This
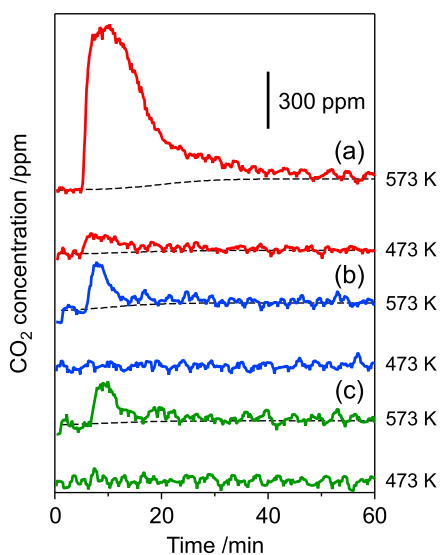
Figure 7. Transient MS responses after the switch He→CO/He (1000 ppm). Catalyst: (a) Rh_4Mo_4/Al_2O_3, (b) $Rh-Mo/Al_2O_3$, and (c) Rh/Al_2O_3.

value is close to 3, which represents the number of oxygen atoms connected to Rh in the precursor $[(RhCp^*)_4Mo_4O_{16}]$, indicating that the Rh/MoO_x interface is derived from the precursor hybrid cluster.

The adsorbed species on the catalyst in a flow of $NO-CO-C_3H_6-O_2$ or $NO-C_3H_6-O_2$ were studied by performing DRIFT analysis. The absorption bands were assigned according to the literature.[23−27] In a flow of $NO-CO-C_3H_6-O_2$, the bands observed for $Rh-Mo/Al_2O_3$ at 473 K were assigned to geminal $Rh^+(CO)_2$ (2101 and 2032 cm^{-1}) and linear $Rh^{2+}-CO$ (2119 cm^{-1}). As the temperature increased, bands assigned to bidentate acetate ($\nu_{as}(OCO)$ 1577 cm^{-1}, $\nu_s(OCO)$ 1461 cm^{-1}) and mononitrosyl $Rh-NO^+$ (1908 cm^{-1}) were observed (Figure 8a). In the case of Rh_4Mo_4/Al_2O_3, the bands assigned to geminal $Rh^+(CO)_2$ (2091 and 2025 cm^{-1}), linear Rh^{2+}-CO (2119 cm^{-1}), and bidentate acetate ($\nu_{as}(OCO)$ 1587 cm^{-1} and $\nu_s(OCO)$ 1468 cm^{-1}) were also observed. No absorption bands assigned to adsorbed NO species were observed. Instead, a prominent peak assigned to isocyanate species bound to the Al site Al−

NCO (2231 with a shoulder at 2250 cm^{-1}) appeared at 573 K. In the flow of $NO-C_3H_6-O_2$, an intense peak assigned to $Rh-NO^+$ was also observed for $Rh-Mo/Al_2O_3$, whereas the intensity of the peak was negligibly small for Rh_4Mo_4/Al_2O_3 (Figure 8b). This trend was also confirmed by the DRIFT spectra of adsorbed species in a flow of NO (Figure S7). No peaks assigned to oxygenated NO species such as $-NO_3$ were observed, except for a broad band of $Rh-Mo/Al_2O_3$ at 473 K (1730−1550 cm^{-1}), which can be attributed to either oxygenated NO or partially oxidized C_3H_6 species. Al−NCO was also observed on Rh_4Mo_4/Al_2O_3, with a much lower intensity than that in the flow of $NO-CO-C_3H_6-O_2$. According to the mechanism of the NO−CO reaction over PGM catalysts,[2,28,29] NO reduction occurs because of the N−O cleavage of adsorbed NO, leaving atomic nitrogen and oxygen on the surface. The formation of N_2 occurs via the coupling of two nitrogen atoms. CO contributed to the removal of atomic oxygen from the surface. Because these reactions take place on reduced metal sites, the reducibility of the metal site is an essential factor for the NO−CO reaction. The N−O cleavage is regarded as the rate-determining step in Rh catalysts, and Rh−NO species are typically observed. Therefore, the absence of −NO species on Rh_4Mo_4/Al_2O_3 implies a significant difference in the reaction mechanism or rate-determining step. The absence of −NO species and the presence of −NCO species on Rh_4Mo_4/Al_2O_3 imply two possibilities for the origin of the improved activity. One possibility is that N−O cleavage on Rh_4Mo_4/Al_2O_3 in the presence of CO is much faster than that of typical Rh catalysts. Rh_4Mo_4/Al_2O_3 showed improved reducibility compared to typical Rh catalysts (Figure 7), which is beneficial for N−O cleavage of adsorbed NO. In addition, the intensity of the peak assigned to Al−NCO after exposure to $NO-CO-C_3H_6-O_2$ was much higher than that of $NO-C_3H_6-O_2$, implying that the Al−NCO species were mainly derived from CO. Adsorbed −NCO can be formed by the reaction of adsorbed CO with atomic nitrogen formed by N−O cleavage of adsorbed NO.[30] This consideration supports the possibility that adsorbed NO was quickly consumed by N−O cleavage on the Rh/MoO_x interfacial site in the presence of CO.

The second possibility is that the $NO-C_3H_6-O_2$ reaction proceeded via a mechanism similar to that of the base metal oxide catalysts, which is different from that of the PGM
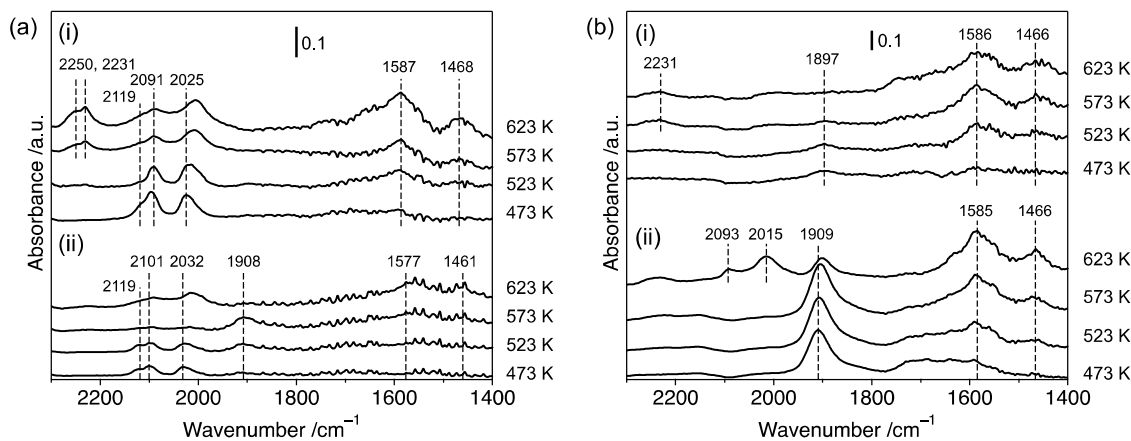
Figure 8. DRIFT spectra of adsorbed species in a flow of (a) $NO-CO-C_3H_6-O_2$ and (b) $NO-C_3H_6-O_2$ on (i) Rh_4Mo_4/Al_2O_3 and (ii) $Rh-Mo/Al_2O_3$. Gas composition: (a) NO (1000 ppm), CO (1000 ppm), C_3H_6 (250 ppm), and O_2 (1125 ppm); (b) NO (1000 ppm), C_3H_6 (250 ppm), and O_2 (625 ppm) balanced with He.
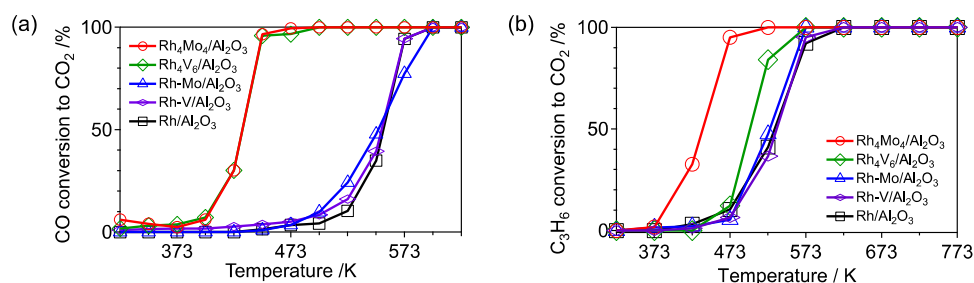
Figure 9. (a) CO conversion to CO_2 in the $CO-O_2$ reaction and (b) C_3H_6 conversion to CO_2 in the $C_3H_6-O_2$ reaction over as-prepared catalysts. Reaction condition: catalyst ((a) 100 mg and (b) 200 mg) and total flow rate (100 mL min^{-1}). Gas composition: (a) CO (1000 ppm) and O_2 (500 ppm); (b) C_3H_6 (250 ppm) and O_2 (1125 ppm) balanced with He.

catalysts. The absence of adsorbed NO leads to a mechanism where NO adsorption is not required. In contrast to PGM catalysts, where the reaction proceeds through N−O cleavage of adsorbed NO, the reaction mechanism proposed for base metal oxide catalysts involves the nitrate species NO_x formed from NO and O_2.[31−35] The partially oxidized species of C_3H_6, such as aldehydes and acetates, were formed on the surface, which contributed to the formation of the reduced form of nitrogen, such as −NCO. The formation of N_2 occurs by the reaction between oxidized (e.g., NO(g), −NO_x) and reduced (e.g.,−NCO) nitrogen compounds. The absence of adsorbed NO_x implied that the reduced nitrogen species on the surface reacted with gaseous or weakly adsorbed NO_x species. The partial oxidation of C_3H_6 proceeds via abstraction of α-hydrogen followed by the insertion of oxygen to an allylic C−H bond.[36] As reported for Bi−Mo-based oxides, practical catalysts for the partial oxidation of C_3H_6 to acrolein, the lattice oxygen atoms are involved in the reaction in the oxygen insertion process[37,38] and the active sites are most probably Bi−O−Mo-containing phases.[39,40] Therefore, we conclude that the oxygen atoms in Rh/MoO_x interfacial sites on Rh_4Mo_4/Al_2O_3 would contribute to the partial oxidation of C_3H_6 to provide the reduced nitrogen species efficiently. The presence of Al−NCO in the $NO-C_3H_6-O_2$ flow supports the hypothesis that the reaction proceeds via the −NCO intermediate. Because C_3H_6 is responsible for NO reduction in the $NO-CO-C_3H_6-O_2$ reaction (Figure S6), we expect that the reducibility of the Rh/MoO_x interfacial site plays an essential role in the partial oxidation of C_3H_6 rather than the formation of oxygen vacancies being beneficial for N−O cleavage.

The origin of the durability of Rh_4Mo_4/Al_2O_3 can also be attributed to the difference in the reaction mechanism. The thermal stabilities of PGM catalysts have been improved by metal−support interactions.[6−8] The presence of strong M^1−O−M^2 interfacial bonding, where M^1 and M^2 represent the PGM and cationic elements in the support, respectively, prevents the active phase from being sintered. However, this also negatively impacts the activity. Although the metallic phase was more active than the oxidized phase, these interactions stabilized the oxidized phase rather than the metallic phase. In addition, the deactivation of Rh catalysts on γ-Al_2O_3 has been explained by the encapsulation of Rh and the formation of inactive rhodium−aluminate $RhAlO_x$ induced by the strong interactions between Rh and γ-Al_2O_3.[41−43] Therefore, the active phases should be stabilized without losing the reducibility.[7,8] In contrast, according to the NO reduction mechanism on Rh_4Mo_4/Al_2O_3, the presence of reduced Rh is less important than that of typical PGM catalysts. We conclude

that the durability of Rh_4Mo_4/Al_2O_3 originates from the formation of thermally stable interfacial Rh/MoO_x sites, where the presence of reduced Rh is not required for the reaction to progress.

To elucidate the different effects of Mo from V, the activities of the $CO-O_2$ and $C_3H_6-O_2$ reactions were also studied. Both Rh_4Mo_4/Al_2O_3 and Rh_4V_6/Al_2O_3 showed higher activities in the $CO-O_2$ reaction than the reference catalysts, regardless of the type of secondary metal (Figure 9a). The formation of single-atomic or highly dispersed metal sites has been reported to be beneficial for CO oxidation.[44,45] According to DRIFT measurements of adsorbed CO on Rh_4Mo_4/Al_2O_3, Rh is highly dispersed in Rh−Mo mixed nanoparticles (Figure 4a). Therefore, we concluded that a high-density of Rh/MO_x interface was formed regardless of the type of secondary metal (M = Mo, V), and the isolated Rh species at the interface were responsible for the reaction.

Although Rh_4Mo_4/Al_2O_3 also showed high activity in the $C_3H_6-O_2$ reaction, slight improvement in activity was observed for Rh_4V_6/Al_2O_3 (Figure 9b). As mentioned earlier, the initial step of C_3H_6 is the abstraction of α-hydrogen and the insertion of oxygen into an allylic C−H bond.[36] The oxygen atoms in the Rh/MoO_x interfacial site on Rh_4Mo_4/Al_2O_3 participate in the oxygen insertion process. The high activity of Rh_4Mo_4/Al_2O_3 in the $C_3H_6-O_2$ reaction supports this mechanism. Therefore, the low activity of Rh_4V_6/Al_2O_3 suggests that the oxygen atoms at the Rh/VO_x interfacial site do not contribute to the oxygen insertion process. This may also affect durability. In contrast to Rh_4Mo_4/Al_2O_3, the activity of Rh_4V_6/Al_2O_3 decreased substantially after thermal aging (Figure 5b). This may be due to the absence of surface oxygen atoms, which contribute to the partial oxidation of C_3H_6 in the case of Rh_4V_6/Al_2O_3.

The introduction of Mo to TWC catalysts has received attention because partially reduced Mo oxide species chemisorb NO to form geminal-dinitrosyl $Mo(NO)_2$, which contributes to the formation of N_2.[2,46] The formation of the interfacial site of PMG with Mo is accomplished using a large excess of Mo, covering the entire surface of the support. However, this approach was impractical because of the high vapor pressure of MoO_3, which volatilizes at above 873−1073 K under oxidizing conditions.[46] To avoid volatilization, composite sites must be prepared at a relatively low loading (<10 wt %).[2,47] According to ICP-MS analysis, the relative ratio of the loading amount (Mo/Rh) was retained after aging, suggesting that the volatilization of Mo was negligible (Table S3). A slight increase in both the Rh and Mo contents was observed for both Rh_4Mo_4/Al_2O_3 and Rh−Mo/Al_2O_3 after aging. This is due to the loss of crystalline water in the support.

We therefore expect that catalyst preparation by hybrid clustering can be a practical method for forming interfacial sites in situations where the use of a large excess of precursors is unfavorable.

3. CONCLUSIONS

To form a high density of metal/oxide interfacial active sites, we prepared catalysts by employing hybrid clustering. A Rh−Mo hybrid cluster $[(RhCp^*)_4Mo_4O_{16}]$ was applied as the catalyst precursor to prepare the hybrid clustering catalyst, Rh_4Mo_4/Al_2O_3, affording composite nanoparticles of Rh and Mo. According to the adsorption behavior of CO, the local structure of Rh was different from that of the coimpregnated Rh−Mo catalyst. Rh−Mo catalysts were used for the NO−CO−C_3H_6−O_2 reaction, wherein their activities depended on the mixing method (hybrid clustering > coimpregnation ≈ pristine Rh). The hybrid clustering catalyst exhibited high durability against thermal aging at 1273 K in air. This is in sharp contrast to the coimpregnated catalyst, whose activity significantly decreased after thermal aging. The activity and durability of Rh_4Mo_4/Al_2O_3 were attributed to the formation of a high density of Rh/MoO_x interfacial sites. The formation of CO_2 under CO/He flow indicated the ease of oxygen vacancy formation. The absence of adsorbed NO on Rh_4Mo_4/Al_2O_3 in the NO−CO−C_3H_6−O_2 flow implied that the NO reduction mechanism on Rh_4Mo_4/Al_2O_3 was different from that of typical PGM catalysts, where the key step is the N−O cleavage of adsorbed NO. The reducibility of the Rh/MoO_x interfacial sites contributed to the partial oxidation of C_3H_6 to form acetate species, which reacted with NO+O_2 to form N_2 via adsorbed NCO. The formation of reduced Rh on Rh_4Mo_4/Al_2O_3 was not as essential as that on typical PGM catalysts; this explains the improvement in durability.

4. EXPERIMENTAL SECTION

4.1. Catalyst Preparation

The hybrid clusters $[(RhCp^*)_4Mo_4O_{16}]$ and $[(RhCp^*)_4V_6O_{19}]$ were synthesized as per a procedure mentioned in the literature[16,17] and characterized by employing FT-IR and ^1H and $^{13}C\{^1H\}$ NMR. The hybrid clustering catalyst Rh_4Mo_4/Al_2O_3, was prepared as follows. $[(RhCp^*)_4Mo_4O_{16}]$ (19.3 mg, 12.1 μmol) was dissolved in methanol (20 mL), and the solution was added dropwise to a methanolic dispersion of the γ-Al_2O_3 support (490 mg in 40 mL). The mixture was stirred for 2 h and then dried slowly at 373 K. The solid was then dried overnight at 353 K. The catalyst was obtained by performing calcination under air flow at 773 K for 1 h. Rh_4V_6/Al_2O_3 was prepared using $[(RhCp^*)_4V_6O_{19}]$ as the precursor. Rh−Mo/Al_2O_3, Rh−V/Al_2O_3, and Rh/Al_2O_3 were prepared using the following precursors: $RhCl_3$, $(NH_4)_6[Mo_7O_{24}]\cdot4H_2O$, and NH_4VO_3. Water was used as the solvent, instead of methanol. The calculated loading amounts of Rh, Mo, and V were 1.0, 0.93, and 0.74 wt %, respectively (Mo/Rh = 1, V/Rh = 1.5).

4.2. Characterization

NMR analysis was conducted using JEOL JNM-ECS400 (400 MHz (^1H), 100 MHz (^{13}C)). $CDCl_3$ was used as the solvent and the chemical shifts were calibrated using tetramethyl silane (^1H) or $CDCl_3$ (^{13}C, δ 77.0 ppm). FT-IR analysis was conducted using a JASCO FT/IR-4200 in transmission mode. The sample was mixed well with KBr and pressed to form a pellet, which was then used for analysis. HAADF-STEM and EDS analyses were conducted using a JEOL JEM-2800 equipped with a silicon drift detector. The sample was prepared by dropping a methanolic dispersion of the catalyst onto a copper grid with a support membrane and evaporating the solvent. The Mo K-edge and Rh K-edge XAS measurements were conducted

using the BL01B1 beamline at SPring-8 of the Japan Synchrotron Radiation Research Institute. The incident X-ray beam was monochromatized by using a Si(311) double-crystal monochromator. The measurements were conducted in fluorescence mode using a 19-element Ge solid-state detector at room temperature. The reference samples were ground well with boron nitride and pressed to form pellets. The XAS data were analyzed by utilizing the Rigaku REX2000 program. Inductively coupled plasma mass spectrometry (ICP-MS) analysis was performed by using an Agilent 7700x instrument. In an autoclave, the catalyst (ca. 50 mg) was digested with 6 mL of aq. H_2SO_4 (50% v/v) at 453 K for 18 h. The samples were then diluted with 1 M aq. HNO_3, and ^{115}In solution was added as an internal standard. Diffused reflectance infrared Fourier transform (DRIFT) spectra were recorded on a JASCO FT/IR-4200 spectrometer equipped with a mercury−cadmium−tellurium (MCT) detector cooled with liquid N_2. The DRIFT spectra of the adsorbed CO were measured as follows: The catalysts (ca. 30 mg) were pretreated with He (50 mL min^{-1}) at 773 K for 30 min and cooled to room temperature under He flow. DRIFT spectra were collected after the catalysts were exposed to 20% CO/He gas (50 mL min^{-1}) for 10 min and purged with He for 10 min. *In situ* DRIFT spectra were obtained using the same procedure, except that the reaction gas (total flow rate, 100 mL min^{-1}: NO, 1000 ppm; CO, 1000 ppm; C_3H_6, 250 ppm; O_2, 1125 ppm; He balance) was used.

4.3. Catalytic Test

The catalytic tests were performed in a fixed-bed flow reactor at atmospheric pressure. In a tubular reactor (i.d. 8 mm), 200 mg of the catalyst was placed and pretreated with He (50 mL min^{-1}) at 773 K for 1 h and cooled to room temperature under He flow. A total flow rate of 100 mL min^{-1} of reaction gas was introduced (gas hourly space velocity, GHSV ~ 15,000 h^{-1}) with a composition of NO (1000 ppm), CO (1000 ppm), C_3H_6 (250 ppm), and O_2 (1125 ppm) balanced with He (stoichiometric condition, λ = 1). The reactor was heated from 373 to 773 K in a stepwise manner (50 K intervals). The temperature was maintained for 30 min before the analysis. The effluent gas was analyzed by using two gas chromatographs (Shimadzu GC-8A, Porapak Q and MS-5A columns) equipped with thermal conductivity detectors and a NO_x analyzer (Anatec Yanaco ECL-88A Lite).

■ ASSOCIATED CONTENT

Ⓢ Supporting Information

The Supporting Information is available free of charge at https://pubs.acs.org/doi/10.1021/acsmaterialsau.3c00001.

Synthesis of hybrid clusters; results of characterization; and catalytic tests (PDF)

■ AUTHOR INFORMATION

Corresponding Authors

Shun Hayashi − *Division of Physical Sciences, Department of Science and Engineering, National Museum of Nature and Science, Ibaraki 305-0005, Japan;* Ⓞ orcid.org/0000-0003-4832-3768; Email: s-hayashi@kahaku.go.jp

Tetsuya Shishido − *Department of Applied Chemistry for Environment, Graduate School of Urban Environmental Sciences, Tokyo Metropolitan University, Tokyo 192-0397, Japan; Research Center for Hydrogen Energy-Based Society, Tokyo Metropolitan University, Tokyo 192-0397, Japan; Elements Strategy Initiative for Catalysts & Batteries, Kyoto University, Kyoto 615-8520, Japan;* Ⓞ orcid.org/0000-0002-8475-4226; Email: shishido-tetsuya@tmu.ac.jp

Authors

Shinji Endo − *Department of Applied Chemistry for Environment, Graduate School of Urban Environmental*

Sciences, Tokyo Metropolitan University, Tokyo 192-0397, Japan

Hiroki Miura − *Department of Applied Chemistry for Environment, Graduate School of Urban Environmental Sciences, Tokyo Metropolitan University, Tokyo 192-0397, Japan; Research Center for Hydrogen Energy-Based Society, Tokyo Metropolitan University, Tokyo 192-0397, Japan; Elements Strategy Initiative for Catalysts & Batteries, Kyoto University, Kyoto 615-8520, Japan;* ⊙ orcid.org/0000-0002-2488-4432

■ REFERENCES

(1) Taylor, K. C. Nitric Oxide Catalysis in Automotive Exhaust Systems. *Catal. Rev.* **1993**, *35*, 457−481.

(2) Shelef, M.; Graham, G. W. Why Rhodium in Automotive Three−Way Catalysts? *Catal. Rev.* **1994**, *36*, 433−457.

(3) Farrauto, R. J.; Heck, R. M. Catalytic Converters: State of the Art and Perspectives. *Catal. Today* **1999**, *51*, 351−360.

(4) Farrauto, R. J.; Deeba, M.; Alerasool, S. Gasoline Automobile Catalysis and Its Historical Journey to Cleaner Air. *Nat. Catal.* **2019**, *2*, 603−613.

(5) Nishihata, Y.; Mizuki, J.; Akao, T.; Tanaka, H.; Uenishi, M.; Kimura, M.; Okamoto, T.; Hamada, N. Self−Regeneration of a Pd−Perovskite Catalyst for Automotive Emissions Control. *Nature* **2002**, *418*, 164−167.

(6) Nagai, Y.; Hirabayashi, T.; Dohmae, K.; Takagi, N.; Minami, T.; Shinjoh, H.; Matsumoto, S. Sintering Inhibition Mechanism of Platinum Supported on Ceria−Based Oxide and Pt−Oxide−Support Interaction. *J. Catal.* **2006**, *242*, 103−109.

(7) Machida, M. Rh Nanoparticle Anchoring on Metal Phosphates: Fundamental Aspects and Practical Impacts on Catalysis. *Chem. Rec.* **2016**, *16*, 2219−2231.

(8) Jeong, H.; Kwon, O.; Kim, B.−S.; Bae, J.; Shin, S.; Kim, H.−E.; Kim, J.; Lee, H. Highly Durable Metal Ensemble Catalysts with Full Dispersion for Automotive Applications beyond Single−Atom Catalysts. *Nat. Catal.* **2020**, *3*, 368−375.

(9) Force, C.; Belzunegui, J. P.; Sanz, J.; Martínez−Arias, A.; Soria, J. Influence of Precursor Salt on Metal Particle Formation in Rh/CeO$_2$ Catalysts. *J. Catal.* **2001**, *197*, 192−199.

(10) Lin, S.; Yang, X.; Yang, L.; Zhou, R. Three−Way Catalytic Performance of Pd/Ce$_{0.67}$Zr$_{0.33}$O$_2$−Al$_2$O$_3$ Catalysts: Role of the Different Pd Precursors. *Appl. Surf. Sci.* **2015**, *327*, 335−343.

(11) Baylet, A.; Royer, S.; Marécot, P.; Tatibouët, J. M.; Duprez, D. Effect of Pd Precursor Salt on the Activity and Stability of Pd−Doped Hexaaluminate Catalysts for the CH$_4$ Catalytic Combustion. *Appl. Catal., B* **2008**, *81*, 88−96.

(12) Hayashi, S.; Shishido, T. High−Density Formation of Metal/ Oxide Interfacial Catalytic Active Sites through Hybrid Clustering. *ACS Appl. Mater. Interfaces* **2021**, *13*, 22332−22340.

(13) Putaj, P.; Lefebvre, F. Polyoxometalates Containing Late Transition and Noble Metal Atoms. *Coord. Chem. Rev.* **2011**, *255*, 1642−1685.

(14) Takahashi, K.; Yamaguchi, M.; Shido, T.; Ohtani, H.; Isobe, K.; Ichikawa, M. Molecular Modelling of Supported Metal Catalysts: SiO$_2$−Grafted $[\{(\eta^3−C_4H_7)_2Rh\}_2V_4O_{12}]$ and $[\{Rh(C_2Me_5)\}_4V_6O_{19}]$ Are Catalytically Active in the Selective Oxidation of Propene to Acetone. *J. Chem. Soc. Chem. Commun.* **1995**, 1301−1303.

(15) Ichikawa, M.; Pan, W.; Imada, Y.; Yamaguchi, M.; Isobe, K.; Shido, T. Surface−Grafted Metal Oxide Clusters and Metal Carbonyl Clusters in Zeolite Micropores; XAFS/FTIR/TPD Characterization and Catalytic Behavior. *J. Mol. Catal. A Chem.* **1996**, *107*, 23−38.

(16) Hayashi, Y.; Toriumi, K.; Isobe, K. Novel Triple Cubane−Type Organometallic Oxide Clusters: $[MCp^*MoO_4]_4•nH_2O$ (M = Rh and Ir; Cp* = C$_5$Me$_5$; n = 2 for Rh and 0 for Ir). *J. Am. Chem. Soc.* **1988**, *110*, 3666−3668.

(17) Hayashi, Y.; Ozawa, Y.; Isobe, K. Site−Selective Oxygen Exchange and Substitution of Organometallic Groups in an Amphiphilic Quadruple−Cubane−Type Cluster. Synthesis and Molecular Structure of $[(MCp^*)_4V_6O_{19}]$ (M = Rh, Ir). *Inorg. Chem.* **1991**, *30*, 1025−1033.

(18) Yamamoto, T. Assignment of Pre−Edge Peaks in K-Edge x−Ray Absorption Spectra of 3d Transition Metal Compounds: Electric Dipole or Quadrupole? *X-Ray Spectrom.* **2008**, *37*, 572−584.

(19) Shishido, T.; Asakura, H.; Yamazoe, S.; Teramura, K.; Tanaka, T. Structural Analysis of Group V, VI, VII Metal Compounds by XAFS and DFT Calculation. *J. Phys. Conf. Ser.* **2009**, *190*, 012073.

(20) Yates, J. T.; Duncan, T. M.; Worley, S. D.; Vaughan, R. W. Infrared Spectra of Chemisorbed CO on Rh. *J. Chem. Phys.* **1979**, *70*, 1219−1224.

(21) Cavanagh, R. R.; Yates, J. T. Site Distribution Studies of Rh Supported on Al$_2$O$_3$ − An Infrared Study of Chemisorbed CO. *J. Chem. Phys.* **1981**, *74*, 4150−4155.

(22) Lang, R.; Li, T.; Matsumura, D.; Miao, S.; Ren, Y.; Cui, Y.−T.; Tan, Y.; Qiao, B.; Li, L.; Wang, A.; Wang, X.; Zhang, T. Hydroformylation of Olefins by a Rhodium Single−Atom Catalyst with Activity Comparable to RhCl(PPh$_3$)$_3$. *Angew. Chem., Int. Ed.* **2016**, *55*, 16054−16058.

(23) Kondarides, D. I.; Chafik, T.; Verykios, X. E. Catalytic Reduction of NO by CO over Rhodium Catalysts: 2. Effect of Oxygen on the Nature, Population, and Reactivity of Surface Species Formed under Reaction Conditions. *J. Catal.* **2000**, *191*, 147−164.

(24) Halkides, T. I.; Kondarides, D. I.; Verykios, X. E. Mechanistic Study of the Reduction of NO by C$_3$H$_6$ in the Presence of Oxygen over Rh/TiO$_2$ Catalysts. *Catal. Today* **2002**, *73*, 213−221.

(25) Flores-Moreno, J. L.; Delahay, G.; Figueras, F.; Coq, B. DRIFTS Study of the Nature and Reactivity of the Surface Compounds Formed by Co−Adsorption of NO, O$_2$ and Propene on Sulfated Titania−Supported Rhodium Catalysts. *J. Catal.* **2005**, *236*, 292−303.

(26) Haneda, M.; Shinoda, K.; Nagane, A.; Houshito, O.; Takagi, H.; Nakahara, Y.; Hiroe, K.; Fujitani, T.; Hamada, H. Catalytic Performance of Rhodium Supported on Ceria−Zirconia Mixed Oxides for Reduction of NO by Propene. *J. Catal.* **2008**, *259*, 223−231.

(27) Imai, S.; Miura, H.; Shishido, T. Selective Catalytic Reduction of NO with CO and C$_3$H$_6$ over Rh/NbOPO$_4$. *Catal. Today* **2019**, *332*, 267−271.

(28) Permana, H.; Simon, Ng. K. Y.; Peden, C. H. F.; Schmieg, S. J.; Lambert, D. K.; Belton, D. N. Adsorbed Species and Reaction Rates for NO−CO over Rh(111). *J. Catal.* **1996**, *164*, 194−206.

(29) Chafik, T.; Kondarides, D. I.; Verykios, X. E. Catalytic Reduction of NO by CO over Rhodium Catalysts: 1. Adsorption and Displacement Characteristics Investigated by In Situ FTIR and Transient−MS Techniques. *J. Catal.* **2000**, *190*, 446−459.

(30) Hecker, W. C.; Bell, A. T. Infrared Observations of RhNCO and SiNCO Species Formed during the Reduction of NO by CO over Silica−Supported Rhodium. *J. Catal.* **1984**, *85*, 389−397.

(31) Meunier, F. C.; Breen, J. P.; Zuzaniuk, V.; Olsson, M.; Ross, J. R. H. Mechanistic Aspects of the Selective Reduction of NO by Propene over Alumina and Silver−Alumina Catalysts. *J. Catal.* **1999**, *187*, 493−505.

(32) Shimizu, K. I.; Kawabata, H.; Maeshima, H.; Satsuma, A.; Hattori, T. Intermediates in the Selective Reduction of NO by Propene over Cu−Al$_2$O$_3$ Catalysts: Transient in−Situ FTIR Study. *J. Phys. Chem. B* **2000**, *104*, 2885−2893.

(33) Haneda, M.; Bion, N.; Daturi, M.; Saussey, J.; Lavalley, J. C.; Duprez, D.; Hamada, H. In Situ Fourier Transform Infrared Study of the Selective Reduction of NO with Propene over Ga$_2$O$_3$−Al$_2$O$_3$. *J. Catal.* **2002**, *206*, 114−124.

(34) Burch, R.; Breen, J. P.; Meunier, F. C. A Review of the Selective Reduction of NOx with Hydrocarbons under Lean−Burn Conditions with Non−Zeolitic Oxide and Platinum Group Metal Catalysts. *Appl. Catal., B* **2002**, *39*, 283−303.

(35) Ueda, K.; Ohyama, J.; Satsuma, A. Investigation of Reaction Mechanism of NO−C$_3$H$_6$−CO−O$_2$ Reaction over NiFe$_2$O$_4$ Catalyst. *ACS Omega* **2017**, *2*, 3135−3143.

(36) Grasselli, R. K.; Burrington, J. D. Selective Oxidation and Ammoxidation of Propylene by Heterogeneous Catalysis. *Adv. Cataly.* 1981, *30*, 133−163.

(37) Moro−Oka, Y.; Ueda, W. Multicomponent Bismuth Molybdate Catalyst: A Highly Functionalized Catalyst System for the Selective Oxidation of Olefin. *Adv. Cataly.* 1994, *40*, 233−273.

(38) Keulks, G. W. The Mechanism of Oxygen Atom Incorporation into the Products of Propylene Oxidation over Bismuth Molybdate. *J. Catal.* **1970**, *19*, 232−235.

(39) Burrington, J. D.; Kartisek, C. T.; Grasselli, R. K. Surface Intermediates in Selective Propylene Oxidation and Ammoxidation over Heterogeneous Molybdate and Antimonate Catalysts. *J. Catal.* **1984**, *87*, 363−380.

(40) Bettahar, M. M.; Costentin, G.; Savary, L.; Lavalley, J. C. On the Partial Oxidation of Propane and Propylene on Mixed Metal Oxide Catalysts. *Appl. Catal., A* **1996**, *145*, 1−48.

(41) Wong, C.; McCabe, R. W. Effects of High−Temperature Oxidation and Reduction on the Structure and Activity of Rh/Al$_2$O$_3$ and Rh/SiO$_2$ Catalysts. *J. Catal.* **1989**, *119*, 47−64.

(42) Zhao, B.; Ran, R.; Cao, Y.; Wu, X.; Weng, D.; Fan, J.; Wu, X. Insight into the Effects of Different Ageing Protocols on Rh/Al$_2$O$_3$ Catalyst. *Appl. Surf. Sci.* **2014**, *308*, 230−236.

(43) Li, C. H.; Wu, J.; Getsoian, A. B.; Cavataio, G.; Jinschek, J. R. Direct Observation of Rhodium Aluminate (RhAlO$_x$) and Its Role in Deactivation and Regeneration of Rh/Al$_2$O$_3$ under Three−Way Catalyst Conditions. *Chem. Mater.* **2022**, *34*, 2123−2132.

(44) Jeong, H.; Lee, G.; Kim, B. S.; Bae, J.; Han, J. W.; Lee, H. Fully Dispersed Rh Ensemble Catalyst to Enhance Low−Temperature Activity. *J. Am. Chem. Soc.* **2018**, *140*, 9558−9565.

(45) Beniya, A.; Higashi, S. Towards Dense Single−Atom Catalysts for Future Automotive Applications. *Nat. Catal.* **2019**, *2*, 590−602.

(46) Halasz, I.; Brenner, A.; Shelef, M.; Simon Ng, K. Y. Preparation and Characterization of PdO−MoO$_3$/γ−Al$_2$O$_3$ Catalysts. *Appl. Catal., A* **1992**, *82*, 51−63.

(47) Kummer, J. T. Use of Noble Metals in Automobile Exhaust Catalysts. *J. Phys. Chem. A* **1986**, *90*, 4747−4752.